Results in Materials 30 (2026) 100925

Contents lists available at ScienceDirect

Results in Materials

journal homepage: www.sciencedirect.com/journal/results-in-materials

Mechanical and temporal response of high-coordinated irregular network reinforced composites

Chelsea Fox [a], Kyrillos Bastawros [a], Tommaso Magrini [b,*], Chiara Daraio [a,**]

[a] Division of Engineering and Applied Science, California Institute of Technology, Pasadena, CA, 91125, USA
[b] Department of Mechanical Engineering, Eindhoven University of Technology, 5600MB, Eindhoven, the Netherlands

ARTICLE INFO

Keywords:
Additive manufacturing
Composite materials
Irregular materials
Metamaterials

ABSTRACT

Irregular architected materials offer a wide design space of mechanical properties beyond that of typical periodic architected materials. However, these irregular materials are often completely stochastic, offering little control over the structure-to-property relationships. Here, we show that intentional design of irregular materials, using topology and geometry, leads to control of the mechanical response. We demonstrate this experimentally using additively manufactured two-phase polymer composites, which we generate using a hexagonal virtual growth algorithm (hexa-VGA). The hexa-VGA tessellates a finite set of hexagonal tiles into an irregular network according to coordination number, defined as the average number of connections per network node. In contrast to prior work on the topic of network reinforced composites, the hexa-VGA allows the design of reinforcing architectures characterized by a broader design space, having a coordination number that spans from one to six, representing a purely monodisperse and regular network. The designs generated by the hexa-VGA are then additively manufactured into two-phase materials, with the network being made of a stiff reinforcing phase, while the space enclosed by the network is filled with a soft elastomeric matrix. Through plate tension tests, we show the dependence between the coordination number and the mechanical properties of the polymer composites, and we highlight design pathways to control temporal variations in the fracture response and improve damage tolerance.

1. Introduction

Architected materials offer a wide range of mechanical properties through the careful design of their structure and the choice of their constitutive materials. Truss and shell-based materials, for example, offer a way to achieve high stiffness and strength while maintaining low weight[1–4], while architected composites offer higher toughness than their constitutive bulk materials [5–8]. These materials often rely on periodicity to achieve their properties, with repeating unit cells which can be tessellated to form an effectively bulk material across a range of different length scales [4,7,9,10]. Although periodic architected materials are easier to design, fabricate and analyze [2,3], researchers have recently begun to explore the design space of irregular architected materials [11–23]. These irregular materials are generated using a wide variety of methods, including spinodal decomposition[19–21], Voronoi tessellations [11,22,23], and virtual growth algorithms [24–26], which stochastically arrange sets of tiles into irregular networks. It has been shown that these irregular architected materials can provide desirable mechanical performances, such as superior damage tolerance [27], tailorable stiffness, strength and fracture toughness [16,17,24–26,28], as well as improved energy absorption [18,19].

Although previous publications have highlighted the role of irregularity on the mechanical [17], impact [18] and fracture [16] responses of two-phase architected materials, several gaps still need to be addressed. The tensile behavior of two-phase architected materials reinforced by networks with a high coordination number (exceeding 3) is still to be characterized. Furthermore, reinforcing networks with a high coordination number, defined as the average connections per each node [29,30] provide the perfect platform to study the effect of tile-composition and constituents homogeneity on the final mechanical properties of the materials. In this work, we tackle these open quests in the field of architected materials.

To succeed, we need to further expand the design space of irregular architected materials, leveraging hexagonal virtual growth algorithms

* Corresponding author.
** Corresponding author.
E-mail addresses: t.magrini@tue.nl (T. Magrini), daraio@caltech.edu (C. Daraio).

https://doi.org/10.1016/j.rinma.2026.100925
Received 30 January 2026; Accepted 5 March 2026
Available online 13 March 2026

(hexa-VGA) as a tool to generate irregular network reinforced composites. Inspired by the stochastic assembly of natural structures, the algorithm grows a network from a set of nodes on a hexagonal grid, with up to 6-sided connectivity for each node. The higher degree of possible connectivity allows us to not only study the transition from bending-dominated to stretching-dominated irregular structures, as defined by the Maxwell number [31], but also to use the coordination number as the input parameter to span the design space across ranges that have never been characterized before in similar materials. The hexa-VGA also provides precise control over both the geometry of the system, defined as the shape of structural features enclosed by the reinforcing network, and its topology, defined as the network connectivity. This allows us to decouple the effects of these two parameters on the mechanical response of the materials. We study these effects experimentally, characterizing additively manufactured polymer composites in controlled quasi-static plate tension experiments [17]. Through our work, we demonstrate that the coordination number and its related degree of irregularity prove the key predictors for global scale mechanical properties in irregular architected materials reinforced by high coordination number networks. Building on our findings, we then show how irregularity can be used to control the temporal evolution of fractures and improve damage tolerance in both bending- and stretching-dominated irregular network reinforced composites.

2. Material design, generation and characterization

2.1. Sample generation

We generate our samples using a hexagonal virtual growth algorithm (hexa-VGA), which assembles a network from a set of nodes placed on a hexagonal grid [32]. Each node has up to 6-sided connectivity and the hexa-VGA generates samples by first defining a list of all possible lines in the network which connect the nodes. The hexa-VGA then selects an arbitrary endpoint and uses the input parameter of coordination number, defined as the average number of connections per node, to assign X lines per node with a "positive" status, while the remaining lines are assigned a "negative" status. Once all lines for a given node are assigned, the hexa-VGA removes the endpoint from the list of available nodes, checks if any of the six neighboring endpoints are free endpoints, and repeats the process. If there are no free neighboring endpoints, a random endpoint is selected, and the process continues until all lines have been assigned a status. Given the underlying hexagonal grid and 6-sided connectivity of the network, we can therefore define a set of 63 geometrically or rotationally unique tiles, which tessellate to form continuous networks (Fig. 1a and b).

Using the coordination number as a design parameter for the hexa-VGA, we study a range of networks, from coordination 2X to coordination 6X. To understand the effect of locally-varying geometry and topology on the global mechanical response, we compare homogenous and non-homogenous distributions of network node connectivity (Fig. 1c). Homogeneous (H) networks are composed primarily of tiles of their coordination number, while the non-homogeneous (nH) networks are composed of different tiles, which average to the same coordination number. For example, we study homogeneous networks with coordination 3X composed of only tiles with coordination 3X (H3_3X). We also study non-homogeneous networks with coordination 3X, either composed of 2X and 4X tiles (nH3_24X), or composed of 1X and 5X tiles (nH3_15X). Furthermore, we study homogenous networks with coordination 4X (H4_4X), as well as non-homogeneous networks composed of 3X and 5X tiles (nH4_35X), and of 1X and 5X tiles (nH4_15X). The 3X and 4X coordination samples also mark the transition point from bending-dominated to stretching-dominated 2D lattices, as defined by the Maxwell number [31],

$$M = b - 2j + 3 \qquad \text{[Eq. 1]}$$

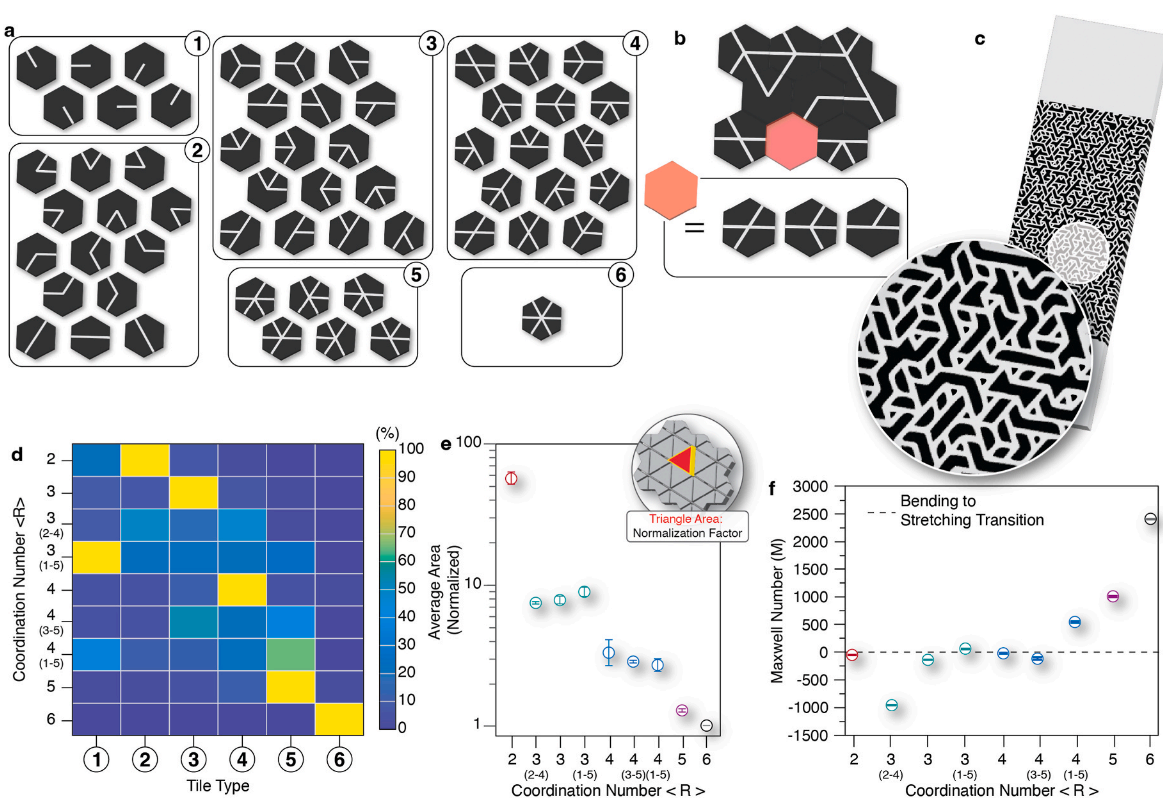

Fig. 1. Hexa-VGA generated sample design and structure characterization. (a) Hexa-VGA tiles. (b) Example of the hexa-VGA network generation. (c) Example of a plate tension sample. (d) Tile distributions for each coordination and topology type. (e) Average area as a function of coordination number. (e) Maxwell number as a function of coordination number.

where b is the number of struts between nodes of coordination 3 or greater, and j is the number of these tiles. It is therefore possible for samples to have the same coordination number and same average structural feature areas (Fig. 1d), while the Maxwell number varies significantly as a result of topological variations (Fig. 1e).

To fabricate our irregular composite materials for testing, we use a Polyjet printer (Stratasys Objet500 Connex3) and we select a stiff viscoelastic resin (VeroWhite Polyjet Resin) for the reinforcing network phase and a soft elastomeric resin (TangoBlack Polyjet Resin) for the matrix phase. Both resins are commercially available, and their constitutive properties fall within ranges reported in literature (Fig. S1) [33–35]. We print the irregular network reinforced composites in samples with a plate tension geometry, with a width of 5 cm, thickness of 3 mm, and a height of 10 cm, with grips of height 3.75 cm. For consistency, we design all samples with 25 hexagonal tiles across and a constant width of the reinforcing network of 0.5 mm, which is an order of magnitude greater than the minimum printer resolution [36]. As a result of maintaining a constant network width, the volume fraction of the different samples increases linearly with increasing coordination, with a value of 0.23 ± 0.001 for 2X samples up to a value of 0.57 ± 0.001 for 6X samples.

2.2. Characterization of the network

To characterize the differences in structure as a result of both coordination number and topology, we first look at how the structural features are arranged. We can define a structural feature by its centroid, which is calculated using regionprops in MATLAB (MathWorks, USA). We can then measure the distribution of these centroids using a radial distribution function (RDF), defined as:

$$g(r) = \frac{\langle \rho(r) \rangle}{\rho_o} \quad \text{[Eq. 2]}$$

where $g(r)$ is the radial density at a radius, r, $\rho(r)$ is the local structural feature density at radius, r, and ρ_o is the feature density of the entire structure (Fig. 2a, inset). We observe that 6X coordination has a periodic radial density, with peaks and valleys at constant intervals, indicative of long-range order [37]. As the coordination number decreases, the structure becomes less ordered, with less distinct frequencies, as a result of the larger design space permitted by the possible structural feature geometries and sizes (Fig. 2a–e, Fig. S2).

We then quantify the distribution of structural feature areas using regionprops in MATLAB (MathWorks, USA). These distributions are effectively a proxy for the Fourier transform of the RDF's, showing the trend of a single frequency for 6X and then wider distributions of frequencies as coordination number decreases (Fig. 2f–n). The distributions also widen as topology becomes more inhomogeneous in iso-coordination samples. This trend can be observed when comparing H3_3X to nH3_24X and to nH3_15X (Fig. 2g–i), as well as when comparing H4_4X to nH4_35X and to nH4_15X (Fig. 2j–l). For comparison, all areas are plotted as triangle normalized, as a triangle formed by connecting three adjacent nodes is the smallest feature that the hexa-VGA can form (Fig. 2o). To summarize these structural feature distribution trends, we then quantify the polydispersity index (PDI) [38,39] of

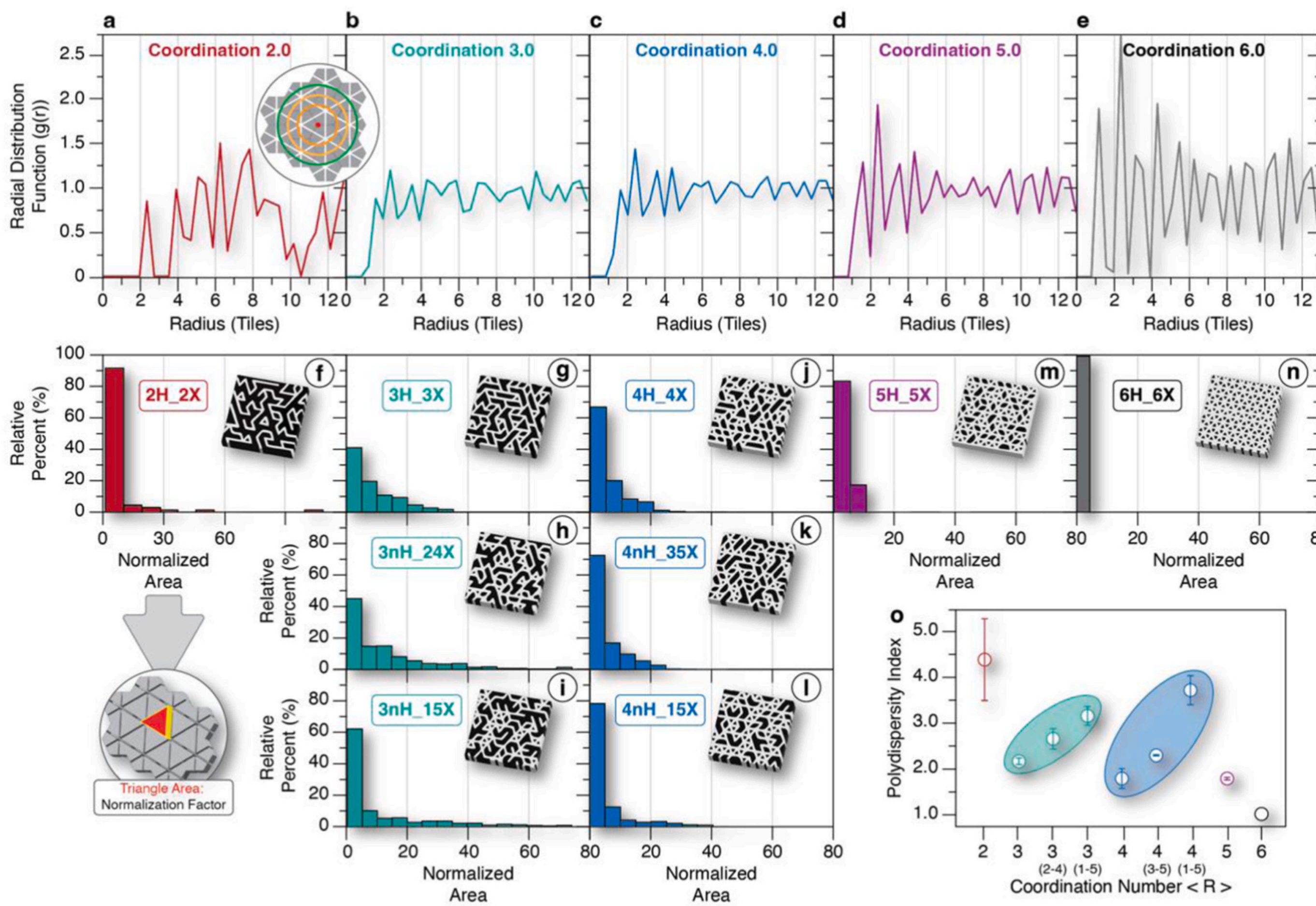

Fig. 2. Geometry characterization of the reinforcing network phase. (a-e) Radial distribution functions for homogeneous coordination samples. (f-n) Structural feature area distributions for all coordination samples in this study. (f, bottom) Example of a triangle normalized area. (o) Polydispersity index (PDI) as a function of the coordination number for all the samples in this study.

the structural feature areas. The PDI indicates the distribution spread of populations of structural features, and its values range from 1 in samples with coordination 6X, where all features are identical, up to 4.3 ± 0.9 for 2X, where the largest possible features can form (Fig. 2p).

3. Results and discussion

3.1. Homogenous topology tensile plate tension tests

We conduct plate tension tests on the composites to understand the effect of coordination number and topology on the mechanical response across the bending to stretching-dominated regimes. We use an Instron E3000 with a 5 kN load cell and fix the samples with clamps at the top and bottom, and then we load the samples at a quasi-static rate of 2 mm/min until failure, defined as the point when samples lose all load bearing capacity.

We first look at the homogeneous topology cases from 2X to 6X. Lower coordination samples show a more ductile response, with larger values of strain-to-failure, while higher coordination samples show lower values of strain-to-failure, but higher strength (Fig. 3a–e). This tradeoff is partly due to the volume fraction of the reinforcing phase, which linearly increases with coordination number, and partly due to the mechanisms of deformation. At lower coordinations (less than 4X), the composites are primarily bending-dominated, while at higher coordinations, the samples are primarily stretching-dominated, and become stiffer and stronger. We also observe that 6X displays a nearly perfect elastic-plastic response, similar to that of the bulk VeroWhite material [17] (Fig. S1), indicating that the reinforcing phase is dominating the response (Fig. 3e). At lower coordinations, even those still in the stretching-dominated regime, the composites are affected by the elastomeric properties of the incompressible matrix material (Fig. S1) displaying a more extensible response and longer time from the first drop in load (as a result of local fractures in the reinforcing network), to complete loss of load-bearing capacity (Fig. 3a–c).

We also conduct 2D digital image correlation (DIC) to understand how strain is accommodated in the materials during loading. We first spray paint the samples with flat white paint and then speckle with flat black paint to achieve an average speckle size of 0.1 to 0.3 mm. We calculate the Lagrangian strain fields using VIC-2D DIC software (Correlated Solutions, USA), with a subset size of 27 and a step size of 2. DIC maps at 2% global strain highlight that the strain becomes more uniformly distributed across the samples with increasing coordination number (Fig. 3f–j). These results agree with the trend quantified by the RDF's, that demonstrated an increased homogeneity in reinforcing network arrangement with increasing coordination (Fig. 2a–e).

Finally, we compare the volume fraction equivalent samples for each coordination to see the effect of different structural arrangements of reinforcing phases (i.e. irregular and periodic). We generate 6H_6X coordination samples with varying structural feature sizes to match the volume fraction of the 2H_2X, 3H_3X, 4H_4X and 5H_5X. These samples (6H_2Vf, 6H_3Vf, 6H_4Vf, 6H_5Vf) show a similar mechanical response to the original 6H_6X samples, as they are stretching-dominated with an elastic-plastic loading profile, followed by a sudden failure and loss of load bearing capacity (Fig. 3k). Unlike the irregular equivalents, these periodic samples do not undergo local failure events with the sawtooth drops in load observed in the irregular equivalents, particularly at higher coordinations, including 4H_4X and 5H_5X. The periodic equivalents also do not reach as high of strain-to-failure values, although this comes at the expense of the ultimate tensile strength, which is higher for the periodic equivalents (Fig. 3k).

3.2. Inhomogeneous topology tensile plate tension tests

We then explore the effect of varying the topology in iso-coordination samples, effectively decreasing the homogeneity of the structures. To achieve this, we test composites with coordination numbers of 3X and 4X, but vary the topology for each, studying 3H_3X, 3 nH_24X, 3 nH_15X, 4H_4X, 4 nH_35X and 4 nH_15X. Due to the variations in topology, the Maxwell number varies significantly, indicating that 3H_3X, 3 nH_24X, 4H_4X and 4 nH_35X are in the bending-dominated regime, while 3X(15) and 4X(15) cross the transition to the stretching-dominated regime (Fig. 1e). We conduct the same plate tension tests as previously described and observe variations in the stress-strain response (Fig. 4a and b). Samples with greater inhomogeneity and greater PDI appear slightly stiffer and stronger, particularly for 3 nH_15X, compared to 3H_3X, and for 4 nH_15X, compared to 4H_4X (Fig. 4a and b, black lines). However, this variation in stiffness is influenced by the volume fraction and by the sample generation method. Indeed, more inhomogeneous topologies result in more constraints during tessellation in the hexa-VGA, as more dissimilar nodes must connect. As a result, nodes grow extra connections to ensure that the sample is one continuous network. This leads to a slightly higher volume fraction of reinforcing phase in the more inhomogeneous samples. These topological variations also cause geometric variations, resulting in more polydisperse structural features, which have the tendency to accommodate strain locally (Fig. 4c–h). To quantify this effect, we measure the modulus of toughness (MOT), defined as the area under the stress-strain curve, expressed in kJ/m^3, indicating the energy the samples can dissipate during rupture, and normalize the MOT by the sample volume fraction. We observe that the normalized MOT correlates linearly with the volume fraction variations across the coordination numbers (Fig. 4i and j), even for bending-dominated composites. This indicates that although the samples accommodate strain differently, the stochastic nature of the irregular network reinforcing phase indicates that the coordination number is the most important parameter for determining the global mechanical response.

3.3. Fracture and temporal response of the composites

We then study the large strain regime, when the materials begin to fracture. In this regime, we investigate the temporal component of the materials' mechanical response to tensile loading as a function of irregularity. We use the image processing software, FIJI, to measure the amount of crack surface opened (Fig. 5a–c) under tensile strain (Fig. 5d–h, Fig. S3), and we observe that coordination number and time-to-failure are inversely related (Fig. 5i). It is important to note that cracks do not initiate at the interface between the two phases, due to their high interfacial toughness [40], but instead nucleate in the matrix phase and then propagate to the reinforcing phase. Lower coordination samples tend to nucleate cracks sooner than higher coordination samples and open a larger amount of total crack area, with as much as 2.38 ± 0.92 times the original cross section opened for 2H_2X (Fig. 5j). This is a result of the bending-dominated response of the network, which can continue to elongate after the adjacent matrix phase fractures, with up to 8.67 ± 0.36 times longer from first crack nucleation to complete loss of load bearing capacity in the samples for 2H_2X when compared with 6H_6X (Fig. 5i).

In contrast, although higher coordination samples also initiate cracks first in the matrix phase and then the reinforcing phase, these samples open up less cross section area, with 5H_5X only opening up 2.07 ± 0.42 times the original cross section of area, while 6H_6X opens up one crack across the entire cross section, although the Poisson ratio reduces this value below the original 300 mm^2 cross section. These higher coordination samples also fail more quickly after the first crack nucleation, with 5H_5X losing all load bearing capacity 1.53 ± 0.09 times faster than 2H_2X, and 1.94 ± 0.41 times faster than 3H_3X. This trend is even more pronounced for the periodic 6H_6X case, which loses all load bearing capacity within just 28.67 ± 2.31 s after crack nucleation, an order of magnitude faster than all other samples (Fig. 5i). This trend for the periodic case is independent of volume fraction, as shown by the equivalent 2X, 3X, 4X and 5X volume fraction samples with 6X coordination (Fig. 5d–h, dashed lines).

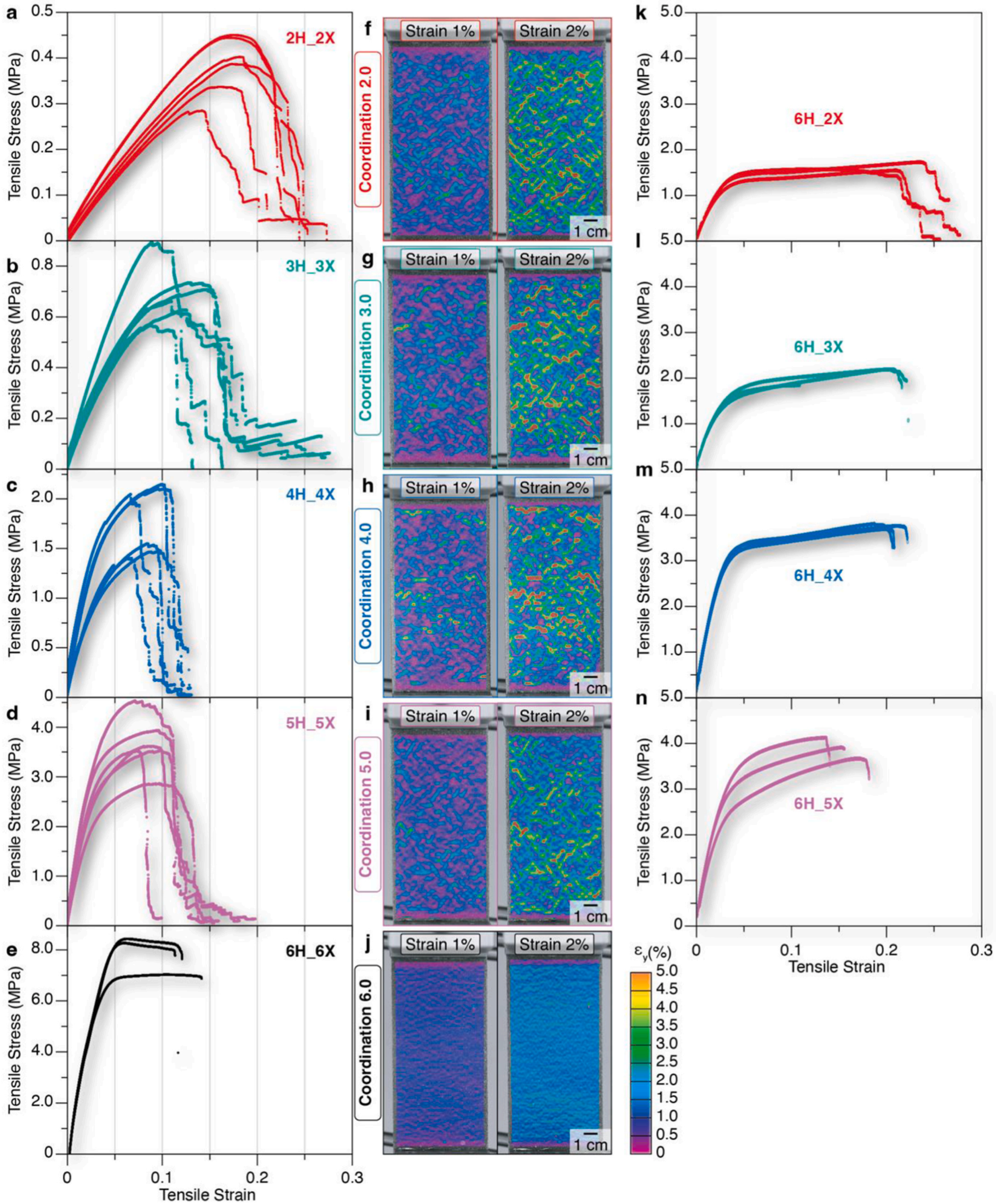

Fig. 3. Tensile testing of irregular network reinforced composites. (a-e) Tensile stress-strain response of 2H_2X, 3H_3X, 4H_4X, 5H_5X and 6H_6X coordination samples. (f-j) Example 2D DIC ε_y strain fields for each sample, comparing frames recorded at 1% and 2% global tensile strain. (k-n) Tensile stress-strain response of 6-coordination samples, having reinforcing phase volume fraction equivalent to the 2H_2X, 3H_3X, 4H_4X and 5H_5X samples, respectively.

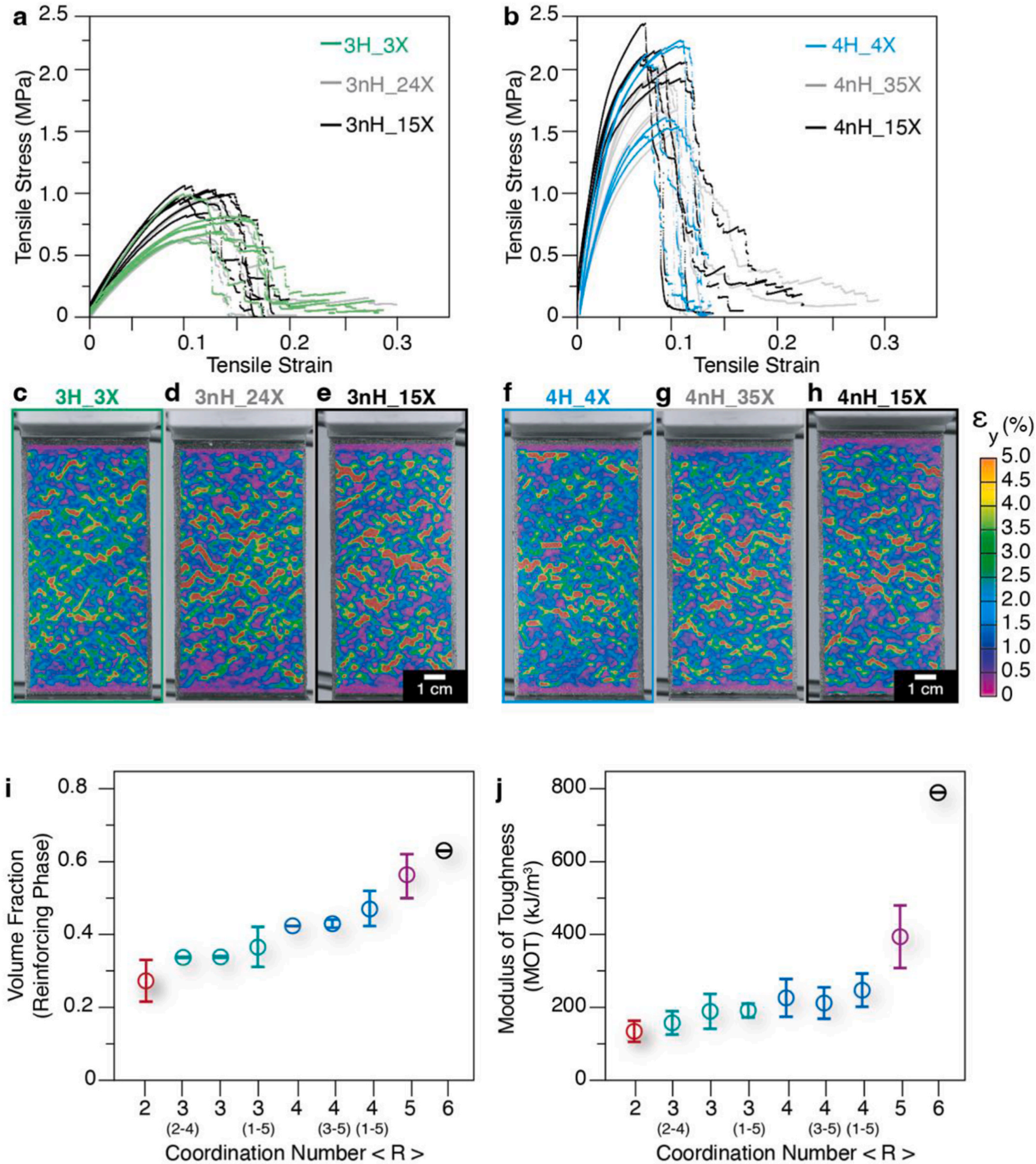

Fig. 4. Characterization of the effect of inhomogeneous topology on irregular network composites. (a) Tensile stress-strain response of 3H_3X, 3 nH_24X and 3 nH_15X samples. (b) Tensile stress-strain response of 4H_4X, 4 nH_35X and 4 nH_15X samples. (c-e) Example 2D DIC ε_y strain fields for 3H_3X, 3 nH_24X and 3 nH_15X samples at 2% global tensile strain. (f-h) Example 2D DIC ε_y strain fields for 4H_4X, 4 nH_35X and 4 nH_15X samples at 2% global tensile strain. (i) Volume fraction of reinforcing phase as a function of coordination number. (j) Modulus of toughness (MOT) (normalized by the volume fraction) as a function of coordination number.

Across both the bending and stretching-dominated regimes, the arrangement of the reinforcing phase into an irregular network instead of a periodic network provides a significant temporal benefit, preventing sudden loss of load bearing capacity. We measure the average crack area opening rate and observe that higher coordinations tend to have a higher rate, with 6H_6X having the fastest rate of nearly 10 mm^2 per second

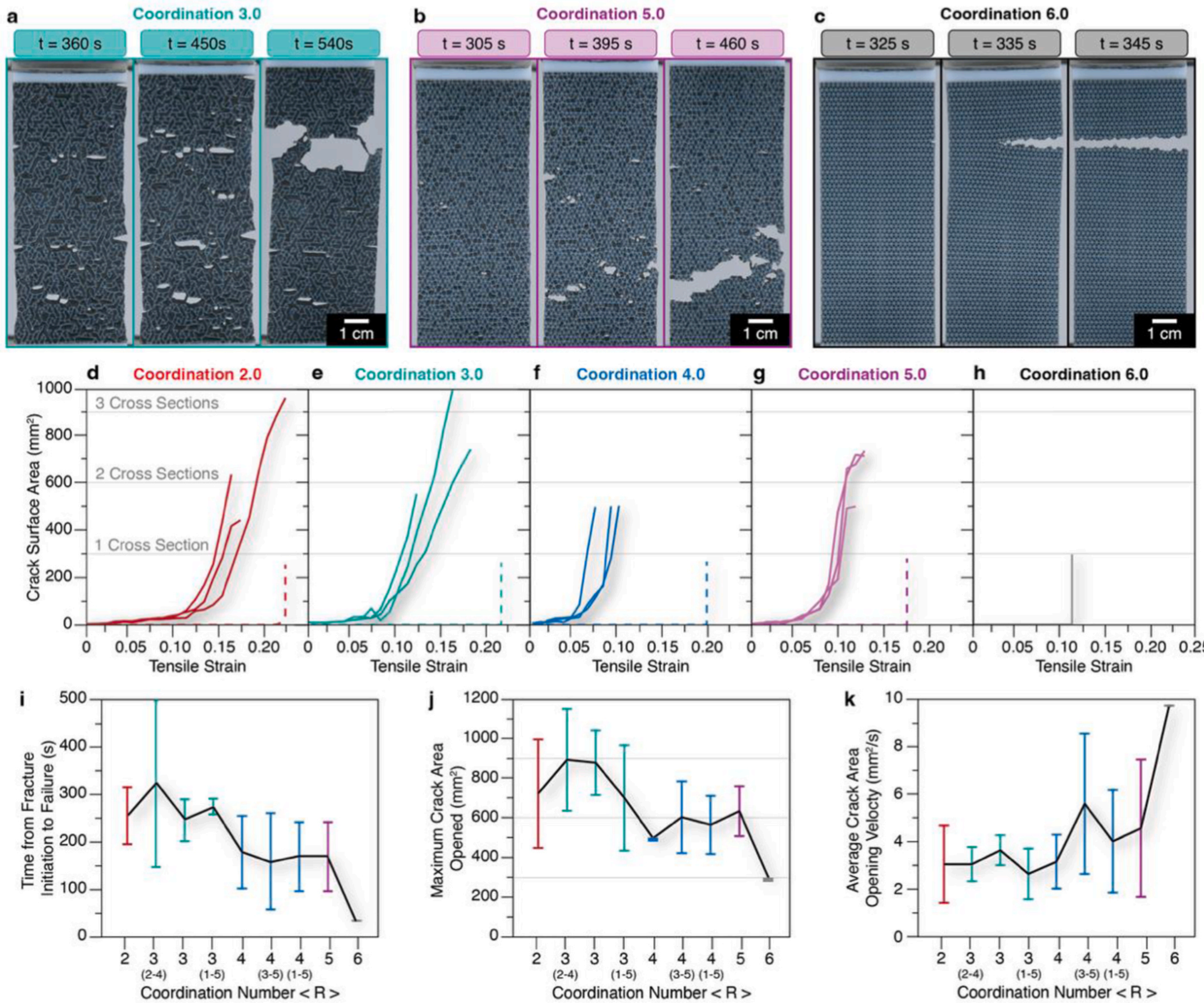

Fig. 5. Temporal characterization of irregular network composite fracture response. (a-c) Time evolution of the crack nucleation and damage propagation in 3H_3X, 5H_5X and 6H_6X composites. (d-h) Crack surface area formed as a function of the applied tensile strain for homogeneous coordination samples. The dashed lines show the periodic volume fraction equivalent 6H_6X samples, as a comparison. (i) Time from fracture initiation to complete loss of load bearing capacity in all samples. (j) Maximum crack area opened. (k) Average crack area opening rate for all samples tested.

(Fig. 5k). This is likely the result of the load bearing pathways in the irregular composites, which reach a wider radius of node connections, creating a more diffuse structural response [41]. In contrast, the periodic equivalents have nodes which are only connected to the nodes closest to themselves. Although these periodic network materials can withstand a higher load, once one node fails, the load bearing capacity drops suddenly and adjacent nodes quickly fail in succession as one crack propagates across the entire sample. The comparison between the periodic and irregular 5X coordination samples demonstrate this best, showing that, although they remain in the stretching-dominated regime, only a small amount of irregularity results in significantly higher strain-to-failure and damage tolerance, as the composites are able to maintain load bearing capacity after crack nucleation and propagation (Fig. 5b and c). Instead of failing suddenly, these samples nucleate many crack locations, with up to 2.95 ± 0.87 times the original cross section of crack surface area distributed across the sample, preventing site coalescence (Fig. 5j).

4. Conclusions

We presented architected network reinforced composite materials and explored the role of irregularity and topology on their mechanical performance. We generated the materials using a hexagonal virtual growth algorithm to achieve control over the topology, using the average network coordination number as an input parameter and varying the local topology to achieve various structural feature polydispersities. We observed that the effect of local topology variations in iso-coordination samples was less influential on the global mechanical response than the average coordination number. We also observed that introducing irregularity leads to improved damage tolerance across both the bending and stretching-dominated regimes. Irregular composites were able to maintain more load bearing capacity even after cracks nucleated and propagated, as the nucleation sites were more dispersed when compared with periodic equivalents. We also showed that this dispersed fracture response leads to variations in the temporal response, which can be controlled as a function of coordination number to achieve an improved mechanical response when compared with periodic equivalents.

CRediT authorship contribution statement

Chelsea Fox: Conceptualization, Investigation, Methodology, Visualization, Writing – original draft, Writing – review & editing. **Kyrillos Bastawros:** Software, Writing – original draft, Writing – review & editing. **Tommaso Magrini:** Conceptualization, Formal analysis, Supervision, Writing – original draft, Writing – review & editing. **Chiara Daraio:** Project administration, Supervision, Writing – original draft, Writing – review & editing.

Declaration of competing interest

The authors declare the following financial interests/personal relationships which may be considered as potential competing interests: Chelsea Fox, Chiara Daraio reports financial support was provided by Multidisciplinary University Research Initiative. If there are other authors, they declare that they have no known competing financial interests or personal relationships that could have appeared to influence the work reported in this paper.

Acknowledgements

The authors thank P. Arakelian for the experimental assistance. C.F. and C.D. acknowledge MURI ARO W911NF-22-2-0109 for the financial support. T. M. acknowledges Dr. R. Style for fruitful discussions.

Appendix A. Supplementary data

Supplementary data to this article can be found online at https://doi.org/10.1016/j.rinma.2026.100925.

Data availability

Data will be made available on request.

References

[1] V.S. Deshpande, M.F. Ashby, N.A. Fleck, Foam topology: bending versus stretching dominated architectures, Acta Mater. 49 (2001) 1035–1040, https://doi.org/10.1016/S1359-6454(00)00379-7.
[2] L.J. Gibson, M.F. Ashby, Mechanics of three-dimensional cellular materials, Proc R Soc Lond A Math Phys Sci 382 (1982) 43–59, https://doi.org/10.1098/RSPA.1982.0088.
[3] L.J. Gibson, M.F. Ashby, G.S. Schajer, C.I. Robertson, The mechanics of two-dimensional cellular materials, Proceedings of the Royal Society of London. A. Mathematical and Physical Sciences 382 (1982) 25–42, https://doi.org/10.1098/RSPA.1982.0087.
[4] M.R. O'Masta, L. Dong, L. St-Pierre, H.N.G. Wadley, V.S. Deshpande, The fracture toughness of octet-truss lattices, J. Mech. Phys. Solid. 98 (2017) 271–289, https://doi.org/10.1016/J.JMPS.2016.09.009.
[5] J. Jung, A. Chen, G.X. Gu, Aperiodicity is all you need: aperiodic monotiles for high-performance composites, Mater. Today (2024), https://doi.org/10.1016/J.MATTOD.2023.12.015.
[6] G.X. Gu, M. Takaffoli, M.J. Buehler, Hierarchically enhanced impact resistance of bioinspired composites, Adv. Mater. 29 (2017), https://doi.org/10.1002/adma.201700060.
[7] T. Magrini, A. Senol, R. Style, F. Bouville, A.R. Studart, Fracture of hierarchical multi-layered bioinspired composites, J. Mech. Phys. Solid. 159 (2022) 104750, https://doi.org/10.1016/J.JMPS.2021.104750.
[8] T. Li, Y. Chen, L. Wang, Enhanced fracture toughness in architected interpenetrating phase composites by 3D printing, Compos. Sci. Technol. 167 (2018) 251–259, https://doi.org/10.1016/J.COMPSCITECH.2018.08.009.
[9] V.S. Deshpande, N.A. Fleck, M.F. Ashby, Effective properties of the octet-truss lattice material, J. Mech. Phys. Solid. 49 (2001) 1747–1769, https://doi.org/10.1016/S0022-5096(01)00010-2.
[10] L.R. Meza, S. Das, J.R. Greer, Strong, lightweight, and recoverable three-dimensional ceramic nanolattices, Science 345 (2014) 1322–1326, https://doi.org/10.1126/SCIENCE.1255908/SUPPL_FILE/MEZA.SM.PDF, 1979.
[11] I. Christodoulou, P.J. Tan, Crack initiation and fracture toughness of random voronoi honeycombs, Eng. Fract. Mech. 104 (2013) 140–161, https://doi.org/10.1016/J.ENGFRACMECH.2013.03.017.
[12] W. Chen, S. Watts, J.A. Jackson, W.L. Smith, D.A. Tortorelli, C.M. Spadaccini, Stiff isotropic lattices beyond the maxwell criterion, Sci. Adv. 5 (2019), https://doi.org/10.1126/SCIADV.AAW1937/SUPPL_FILE/AAW1937_SM.PDF.
[13] S. Fulco, M.K. Budzik, H. Xiao, D.J. Durian, K.T. Turner, Disorder enhances the fracture toughness of 2D mechanical metamaterials, PNAS Nexus 4 (2025), https://doi.org/10.1093/PNASNEXUS/PGAF023.
[14] S. Choukir, N. Manohara, C.V. Singh, Disorder unlocks the strength-toughness trade-off in metamaterials, Appl. Mater. Today 42 (2025) 102579, https://doi.org/10.1016/J.APMT.2024.102579.
[15] W. Deng, S. Kumar, A. Vallone, D.M. Kochmann, J.R. Greer, AI-Enabled materials design of non-periodic 3D architectures with predictable direction-dependent elastic properties, Adv. Mater. 36 (2024) 2308149, https://doi.org/10.1002/ADMA.202308149.
[16] C. Fox, T. Magrini, C. Daraio, Fracture Characterization of Bioinspired Irregular Network Reinforced Composites, (n.d.).
[17] T. Magrini, C. Fox, A. Wihardja, A. Kolli, C. Daraio, Control of mechanical and fracture properties in two-phase materials reinforced by continuous, irregular networks, Adv. Mater. (2023) 2305198, https://doi.org/10.1002/ADMA.202305198.
[18] C. Fox, K. Chen, M. Antonini, T. Magrini, C. Daraio, Extracting geometry and topology of Orange pericarps for the design of bioinspired energy absorbing materials, Adv. Mater. (2024) 2405567, https://doi.org/10.1002/ADMA.202405567.
[19] A. Guell Izard, J. Bauer, C. Crook, V. Turlo, L. Valdevit, A. Guell Izard, J. Bauer, L. Valdevit, C. Crook, V. Turlo, Ultrahigh energy absorption multifunctional spinodal nanoarchitectures, Small 15 (2019) 1903834, https://doi.org/10.1002/SMLL.201903834.
[20] M.T. Hsieh, B. Endo, Y. Zhang, J. Bauer, L. Valdevit, The mechanical response of cellular materials with spinodal topologies, J. Mech. Phys. Solid. 125 (2019) 401–419, https://doi.org/10.1016/J.JMPS.2019.01.002.
[21] Y. Zhang, M.T. Hsieh, L. Valdevit, Mechanical performance of 3D printed interpenetrating phase composites with spinodal topologies, Compos. Struct. 263 (2021) 113693, https://doi.org/10.1016/J.COMPSTRUCT.2021.113693.
[22] G. Wang, L. Shen, J. Zhao, H. Liang, D. Xie, Z. Tian, C. Wang, Design and compressive behavior of controllable irregular porous scaffolds: based on voronoi-tessellation and for additive manufacturing. https://doi.org/10.1021/acsbiomaterials.7b00916, 2018.
[23] K. Karapiperis, D.M. Kochmann, Prediction and control of fracture paths in disordered architected materials using graph neural networks, Commun. Eng. 2 (1 2) (2023) 1–9, https://doi.org/10.1038/s44172-023-00085-0, 2023.
[24] K. Liu, R. Sun, C. Daraio, Growth rules for irregular architected materials with programmable properties, Science 377 (2022) 975–981, https://doi.org/10.1126/SCIENCE.ABN1459/SUPPL_FILE/SCIENCE.ABN1459_MOVIES_S1_TO_S3.ZIP, 1979.
[25] R. Wang, Y. Bian, K. Liu, Nonlinear mechanical properties of irregular architected materials, J. Appl. Mech. (2025) 1–20, https://doi.org/10.1115/1.4067570.
[26] Y. Jia, K. Liu, X.S. Zhang, Unstructured growth of irregular architectures for optimized metastructures, J. Mech. Phys. Solid. 192 (2024) 105787, https://doi.org/10.1016/J.JMPS.2024.105787.
[27] X. Wang, Z. Li, X. Guo, X. Li, Z. Wang, Superior damage tolerance observed in interpenetrating phase composites composed of aperiodic lattice structures, Extreme Mech. Lett. 72 (2024) 102227, https://doi.org/10.1016/J.EML.2024.102227.
[28] Y. Jia, K. Liu, X.S. Zhang, Topology optimization of irregular multiscale structures with tunable responses using a virtual growth rule, Comput. Methods Appl. Mech. Eng. 425 (2024) 116864, https://doi.org/10.1016/J.CMA.2024.116864.
[29] M. Thorpe, P. Duxbury, Rigidity theory and applications, rigidity theory and applications. https://doi.org/10.1007/B115749, 2002.
[30] M.F. Thorpe, Continuous deformations in random networks, J. Non-Cryst. Solids 57 (1983) 355–370, https://doi.org/10.1016/0022-3093(83)90424-6.
[31] J.C. M, F. R, S. L, On the calculation of the equilibrium and stiffness of frames, London, Edinburgh Dublin Phil. Mag. J. Sci. 27 (1864) 294–299, https://doi.org/10.1080/14786446408643668.
[32] C. Fox, K. Bastawros, T. Magrini, C. Daraio, Controllable interlocking from irregularity in two-phase composites. https://arxiv.org/pdf/2502.18392, 2025. (Accessed 28 April 2025).
[33] J.R.C. Dizon, A.H. Espera, Q. Chen, R.C. Advincula, Mechanical characterization of 3D-printed polymers, Addit. Manuf. 20 (2018) 44–67, https://doi.org/10.1016/J.ADDMA.2017.12.002.
[34] D. Bell, T. Siegmund, 3D-printed polymers exhibit a strength size effect, Addit. Manuf. 21 (2018) 658–665, https://doi.org/10.1016/J.ADDMA.2018.04.013.
[35] V. Slesarenko, S. Rudykh, Towards mechanical characterization of soft digital materials for multimaterial 3D-printing, Int. J. Eng. Sci. 123 (2018) 62–72, https://doi.org/10.1016/J.IJENGSCI.2017.11.011.
[36] L. Jiaying Tan, W. Zhu, K. Zhou, L.J. Tan, W. Zhu, K. Zhou, Recent progress on polymer materials for additive manufacturing, Adv. Funct. Mater. 30 (2020) 2003062, https://doi.org/10.1002/ADFM.202003062.

[37] A. Brodin, A. Nych, U. Ognysta, B. Lev, V. Nazarenko, M. Škarabot, I. Muševič, Melting of 2D liquid crystal colloidal structure, Condens. Matter Phys. 13 (2010) 1–12. http://www.icmp.lviv.ua/journal. (Accessed 28 April 2025).
[38] A. Shrivastava, Polymerization, Introduction to Plastics Engineering, 2018, pp. 17–48, https://doi.org/10.1016/B978-0-323-39500-7.00002-2.
[39] R.G. Gilbert, M. Hess, A.D. Jenkins, R.G. Jones, P. Kratochvíl, R.F.T. Stepto, Dispersity in polymer science (IUPAC recommendations 2009), Pure Appl. Chem. 81 (2009) 351–353, https://doi.org/10.1351/PAC-REC-08-05-02/MACHINEREADABLECITATION/RIS.
[40] R.J. Nash, Y. Li, Experimental and numerical analysis of 3D printed suture joints under shearing load, Eng. Fract. Mech. 253 (2021) 107912, https://doi.org/10.1016/J.ENGFRACMECH.2021.107912.
[41] M.M. Driscoll, B.G.G. Chen, T.H. Beuman, S. Ulrich, S.R. Nagel, V. Vitelli, The role of rigidity in controlling material failure, Proc. Natl. Acad. Sci. USA. 113 (2016) 10813–10817, https://doi.org/10.1073/PNAS.1501169113/ASSET/42F87674-24B2-437A-9110-AFC9A626DDA2/ASSETS/GRAPHIC/PNAS.1501169113FIG04.JPEG.